Mathematical Modeling of Solid Oxide Fuel Cells at High Fuel Utilization Based on Diffusion Equivalent Circuit Model

Cheng Bao
Dept. of Thermal Science and Energy Engineering, School of Mechanical Engineering, University of Science and Technology Beijing, Beijing 100083, People's Republic of China, and Key Laboratory for Thermal Science and Power Engineering of Ministry of Education, Tsinghua University, Beijing, 100084, People's Republic of China

Yixiang Shi, Chen Li, and Ningsheng Cai
Key Laboratory for Thermal Science and Power Engineering of Ministry of Education, Tsinghua University, Beijing, 100084, People's Republic of China

Qingquan Su
Dept. of Thermal Science and Energy Engineering, School of Mechanical Engineering, University of Science and Technology Beijing, Beijing 100083, People's Republic of China

DOI 10.1002/aic.12053
Published online September 29, 2009 in Wiley InterScience (www.interscience.wiley.com).

Mass transfer and electrochemical phenomena in the membrane electrode assembly (MEA) are the core components for modeling of solid-oxide fuel cell (SOFC). The general MEA model is simply governed with the Stefan-Maxwell equation for multicomponent gas diffusion, Ohm's law for the charge transfer and the current-overpotential equation for the polarization calculation. However, it has obvious discrepancy at high-fuel utilization or high-current density. An advanced MEA model is introduced based on the diffusion equivalent circuit model. The main purpose is to correct the real-gas concentrations at the triple-phase boundary by assuming that the resistance of surface diffusion is in series with that of the gaseous bulk diffusion. Thus, it can obtain good prediction of cell performance in a wide range by avoiding the decrement of effective gas diffusivity via unreasonable increment of the electrode tortuosity in the general MEA model. The mathematical model has been validated in the cases of H_2—H_2O, CO—CO_2 and H_2—CO fuel system. © 2009 American Institute of Chemical Engineers *AIChE J,* 56: 1363–1371, 2010
Keywords: solid-oxide fuel cell, diffusion equivalent circuit, surface diffusion, high-fuel utilization, mathematical model

Introduction

Fuel cells are electrochemical devices which convert the energy from a chemical reaction directly into electrical energy. Solid-oxide fuel cells (SOFC) is equipped with the high-energy conversion efficiency, less parasitic facilities, high-quality exhaust energy and considerable fuel flexibility, thus, it is considered to be the most potential candidate for distributed power system, power station and automotive applications.

There are complex transfer phenomena and electrochemical/chemical reactions in solid-oxide fuel cells. Modeling

Correspondence concerning this article should be addressed to C. Bao at baocheng@mail.tsinghua.edu.cn

and simulation plays an important role in the development of fuel cell technology. In recent years, many numerical SOFC models have been built for detailed mechanistic analysis. By taking various factors into consideration (including different cell structure, gas flow and heat transfer, radiant heat exchange between solid phases, hydrocarbon fuel internal reforming and gas recycling), the state-of-the-art general cell models have been developed into the multidimensional, nonisothermal and transient ones with the commercial solvers.[1] However, description of the mass transfer and electrochemical phenomena in the membrane electrode assembly (MEA) is the core component of SOFC modeling. In the microelectrode models,[2,3] the cell characteristic properties such as the electrode porosity, tortuosity, conductivity, and the specific active area are related to the electrode particulate composites. In the general MEA model, these estimated characteristic properties play important roles in the calculation of the effective multicomponent gaseous diffusivity, the effective ionic/electronic phase conductivity and the electrochemical reaction rate.[4–8] In the cases of medium-low electric load or medium-low reactant utilization, these macroscopic models were validated well by comparing the estimated data with the experimental cell current-voltage performance.

As a matter of fact, for a practical solid-oxide fuel cell or a staged stack with reasonable overall fuel utilization, the operating condition with low-fuel concentration usually occurs at some local spots. As the fuel is consumed and diluted by the product gradually along the anode flow channel, the fuel concentration decreases at the downstream flow channel in a single cell or the cells near the stack outlet. When the general MEA model is used in the distributed cell or stack modeling, there is obvious discrepancy for the downstream slice units. The overestimation of the general MEA model in the critical conditions results from ignorance of some important mechanisms, such as the surface diffusion and competition absorption/desorption.

On the other hand, some literatures were focused on mechanisms of hydrogen oxidation or oxygen reduction reaction.[9,10,11] Due to the complicated microstructure of conventional Ni-YSZ (yttria-stabilized zirconia) cermet, it is very difficult to isolate the reaction kinetic parameters. Anode kinetic studies were, therefore, carried out on specialized anode assemblies such as Ni pattern electrodes, Ni point electrodes and porous Ni electrodes. Based on the technology of surface science data and electrochemical impedance spectroscopy, the elementary steps of adsorption/desorption, charge transfer and surface reactions were analyzed. Although the complex work earlier is very helpful for the better understanding of physical and chemical phenomena, it is not suitable to be used directly in the high-level modeling.

The purpose of this article is to present an advanced MEA model. It keeps the simple structure of the general MEA model, that is, by using the Stefan-Maxwell equation (or dusty gas model) for the multicomponent gaseous molecular and Kundsen diffusion, Ohm's law for the charge transfer, Butler-Volmer equation for the electrochemical polarization. By introducing a diffusion equivalent circuit model, the multicomponent gaseous surface diffusion and competitive absorption were included, and the complex elementary reaction steps were prevented. Then the species concentrations at the reaction site in the Butler-Volmer equation were corrected to reflect the dominant diffusion resistance in the critical conditions.

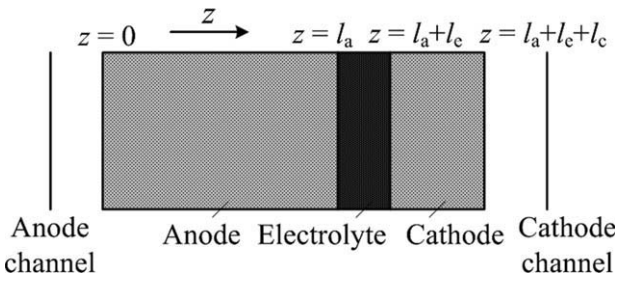

Figure 1. 1-D schematic diagram of MEA in SOFC.

This article is organized as follows. First, we will introduce the general MEA model and its unreasonable correction of effective diffusion resistance in the critical conditions. Second, the diffusion equivalent circuit model is presented. Then the advanced MEA model is validated in different cases of fuel mixture and fuel components. The conclusions are summarized at last.

General MEA model

As shown in Figure 1, the core of SOFC is a "sandwich" structure of MEA. The electrolyte is made of a ceramic such as yttria-stabilized zirconia (YSZ), and plays a role in conducting oxygen ion and separating fuel from oxidant. The material of the anode is typically a Ni-YSZ cermet, and the cathode is mostly lanthanum-based perovskite. Both of the electrodes are formed by a porous mixture of ionic conductor/electronic conductor materials for the gas diffusion and ion/electron transport to make the three-phase boundary (TPB). At the site of TPB, the electrochemical reaction occurs, which is oxidation of fuel ($H_2 + O^{2-} \rightarrow H_2O + 2e^-$, $CO + O^{2-} \rightarrow CO_2 + 2e^-$) in the anode and reduction of oxygen ($1/2\ O_2 + 2e^- \rightarrow O^{2-}$) in the cathode, while the current density exchanges between the ionic and electronic conducting phases. For the small thickness of MEA, the temperature and pressure are assumed to be uniform through out the MEA structure. As shown in Figure 1, only the z coordinate in the thickness direction of MEA is considered here, and the positive direction is from the anode to the cathode. Only steady state is considered in this article.

Governing equations

According to Ohm's law, charge transfer in the electron conducting phase (el) and the ion conducting phase (ion) of the electrode are

$$-\sigma_{\text{ion}}^{\text{eff}}\nabla^2\phi_{\text{ion}} = \sigma_{\text{el}}^{\text{eff}}\nabla^2\phi_{\text{el}} = \sum\nolimits_k \psi j_{\text{k}} \quad (\text{k} = \text{H}_2, \text{CO or O}_2) \tag{1}$$

where φ and σ are the potential, conductivity in electronic phase and ionic phase, respectively, ψ indicates the direction of current flow (i.e., $\psi = 1$ in the anode, and $\psi = -1$ in the cathode), and the electrochemical reaction rate (H_2 and CO oxidation in the anode, oxygen reduction in the cathode), j can be described by the general Bulter-Volmer equation[12]

$$j = i_{0,\mathrm{ref}} S_{\mathrm{TPB}} \exp\left[-\frac{E}{\Re}\left(\frac{1}{T}-\frac{1}{T_{\mathrm{ref}}}\right)\right]\Pi\left(\frac{p_i}{p_0}\right)^{\gamma_i} \left[\frac{c_{\mathrm{react,TPB}}}{c_{\mathrm{react,b}}}\exp\left(\frac{\alpha n_e F}{\Re T}\psi\eta\right) - \frac{c_{\mathrm{prod,TPB}}}{c_{\mathrm{prod,b}}}\exp\left(-\frac{\beta n_e F}{\Re T}\psi\eta\right)\right] \quad (2)$$

where F is the Faraday constant, $\Re$ is the gas constant, T is the operating temperature, n_e is number of electrons participating in the electrochemical reaction, α and β are the charge transfer coefficients, $i_{0,\mathrm{ref}}$ is the reference exchange current density at the reference temperature T_{ref}, E is the activation energy, p_i and γ_i is the partial pressure and reaction order of species i, $c_{\mathrm{react,TPB}}$, $c_{\mathrm{prod,TPB}}$, $c_{\mathrm{react,b}}$, $c_{\mathrm{prod,b}}$ are the reactant and product concentrations at the reaction active sites and bulk concentrations, respectively, and S_{TPB} is the TPB active area per unit volume of electrode, and the overpotential η is defined as the potential difference between the two phases minus the potential difference in equilibrium, which is positive in the anode and negative in the cathode

$$\eta = \phi_{\mathrm{el}} - \phi_{\mathrm{ion}} - (\phi_{\mathrm{el}}^{\mathrm{eq}} - \phi_{\mathrm{ion}}^{\mathrm{eq}}) \quad (3)$$

The mass transfer in the porous electrode is described by Stefan-Maxwell equation

$$-\nabla x_i = \frac{\tau}{\varepsilon_{\mathrm{P}}}\left(\sum_{j=1}^{n}\frac{x_j N_i - x_i N_j}{c_{\mathrm{t}} D_{ij}} + \frac{N_i}{c_{\mathrm{t}} D_{i,\mathrm{K}}}\right) \quad (i = 1, 2, ..., n) \quad (4)$$

where $c_{\mathrm{t}} = p/\Re T$ is the total concentration of gas mixture, x_i and N_i is the molar fraction and diffusion flux of species i, ε_{p} is the electrode porosity, τ is the electrode tortuosity, the calculation of the binary diffusivity between gaseous species i and j (D_{ij}), and the Knudsen diffusion coefficient of species i ($D_{i,\mathrm{K}}$) can be found easily in a textbook.[13]

The mass balance of species in the electrode is related to the electrochemical reaction rate

$$\nabla \cdot N_i = \sum\nolimits_{\mathrm{k}} \upsilon_{\mathrm{elec},k,i} j_{\mathrm{k}}/n_e F + R_i \quad (\mathrm{k} = \mathrm{H_2, CO\ or\ O_2}) \quad (5)$$

where $\upsilon_{\mathrm{elec},i,\mathrm{k}}$ is the stoichiometric coefficient of species i in the electrochemical reaction and R_i is chemical reaction rate of species i. For binary fuel system, $R_i = 0$.

In the electrolyte layer, there is the linear distribution of the ionic phase potential

$$\nabla^2 \phi_{\mathrm{ion}} = 0 \quad (6)$$

Boundary conditions and numeric solution

There are two methods for the calculation of cell polarization performance. One is with the given current density, and the other is with the given cell voltage. Correspondingly, there are two kinds of boundary conditions.

At the flow channel/electrode interface ($z = 0$ or $z = l_{\mathrm{a}}+l_{\mathrm{e}}+l_{\mathrm{c}}$), species concentration is the bulk concentration and the ionic phase current is fully transferred to the electronic phase current ($i_{\mathrm{ion}} = 0$, $i_{\mathrm{el}} = I$). When the operating current density (I) is given, it is

$$x_i|_{z=0,z=l_a+l_e+l_c} = x_{i,\mathrm{b}}, \frac{\mathrm{d}\eta}{\mathrm{d}z}|_{z=0,z=l_a+l_e+l_c} = -\frac{I}{\sigma_{\mathrm{el}}^{\mathrm{eff}}} \quad (7)$$

When the cell voltage (V_{cell}) is given, the electronic phase potential at the anode/flow channel interface is usually set to zero ($\phi_{\mathrm{el}} = 0$), and the electronic potential at the cathode/flow channel interface is equal to the cell voltage ($\phi_{\mathrm{el}} = V_{\mathrm{cell}}$), that is

$$x_i|_{z=0,z=l_a+l_e+l_c} = x_{i,\mathrm{b}}, \frac{\mathrm{d}\phi_{\mathrm{ion}}}{\mathrm{d}z}|_{z=0,z=l_a+l_e+l_c} = 0, \quad \phi_{\mathrm{el}}|_{z=0} = 0, \phi_{\mathrm{el}}|_{z=l_a+l_e+l_c} = V_{\mathrm{cell}} \quad (8)$$

At the electrode/electrolyte interface ($z = l_{\mathrm{a}}$ or $z = l_{\mathrm{a}} + l_{\mathrm{e}}$), the dense electrolyte layer prevents the gases' penetration, and the electronic phase current is fully transferred to the ionic phase current ($i_{\mathrm{ion}} = I$, $i_{\mathrm{el}} = 0$). When the operating current density (I) is given, it is

$$N_i|_{z=l_a,z=l_a+l_e} = 0, \frac{\mathrm{d}\eta}{\mathrm{d}z}|_{z=l_a,z=l_a+l_e} = \frac{I}{\sigma_{\mathrm{ion}}^{\mathrm{eff}}} \quad (9)$$

When the cell voltage is given, the anode/electrolyte and the cathode/electrolyte interface for the ionic phase potential becomes the internal boundary, that is, the ionic phase current through the interface should be continuous considering the continuous distribution of ionic conductor

$$N_i|_{z=l_a,z=l_a+l_e} = 0, \quad \frac{\mathrm{d}\phi_{\mathrm{el}}}{\mathrm{d}z}|_{z=l_a,z=l_a+l_e} = 0, \quad \sigma_{\mathrm{ion,a}}^{\mathrm{eff}}\frac{\mathrm{d}\phi_{\mathrm{ion}}}{\mathrm{d}z}|_{z=l_a}^{-} = \sigma_{\mathrm{ion}}\frac{\mathrm{d}\phi_{\mathrm{ion}}}{\mathrm{d}z}|_{z=l_a}^{+}, \quad \sigma_{\mathrm{ion}}\frac{\mathrm{d}\phi_{\mathrm{ion}}}{\mathrm{d}z}|_{z=l_a+l_e}^{-} = \sigma_{\mathrm{ion,c}}^{\mathrm{eff}}\frac{\mathrm{d}\phi_{\mathrm{ion}}}{\mathrm{d}z}|_{z=l_a+l_e}^{-} \quad (10)$$

When the operating current density is given, there are $2n + 1$ variables for the n species, that is, x_i, N_i and η. This typical boundary problem can be solved by using the standard ***BVP4C*** algorithm in MATLAB. At this time, the anode system and the cathode system can be calculated independently. When the electrode overpotential distribution is calculated, the total overpotential (η_{t}) can be obtained by[12]

$$\eta_{\mathrm{t,k}} = \frac{1}{\sigma_{\mathrm{el,k}}^{\mathrm{eff}} + \sigma_{\mathrm{ion,k}}^{\mathrm{eff}}}\left[\sigma_{\mathrm{ion,k}}^{\mathrm{eff}}\eta_{\mathrm{k}}|_{\mathrm{EC}} + \sigma_{\mathrm{el,k}}^{\mathrm{eff}}\eta_{\mathrm{k}}|_{\mathrm{EE}} + \psi I l_{\mathrm{k}}\right](\mathrm{k} = \mathrm{a, c}) \quad (11)$$

where E/C means the electrode/flow channel interface, E/E means the electrode/electrolyte interface. With the calculated ohmic loss of the electrolyte layer ($\eta_{\mathrm{ohm}} = I l_{\mathrm{e}}\sigma_{\mathrm{ion}}$), the cell voltage can be obtained by

$$V_{\mathrm{cell}} = V_{\mathrm{oc}} - \eta_{\mathrm{t,a}} - |\eta_{\mathrm{t,c}}| - \eta_{\mathrm{ohm}} = V_{\mathrm{oc}} - \eta_{t,a} - |\eta_{\mathrm{t,c}}| - I l_{\mathrm{e}}\sigma_{\mathrm{ion}} \quad (12)$$

where V_{oc} is the open circuit voltage which can be obtained by Nernst equation or the experimental data considering the leakage overpotential.

Table 1. Cell Structural Parameters and Operating Conditions in Base Case

Parameter	Symbol	Value
Anode thickness (m)	l_a	1.1×10^{-3}
Electrolyte layer thickness (m)	l_e	1.0×10^{-5}
Cathode thickness (m)	l_c	6.0×10^{-5}
Anode pressure (bar)	p_a	1.0
Cathode pressure (bar)	p_c	1.0
Cell temperature (K)	T	1073.15
Fuel components		85%H_2–15%H_2O

When the cell voltage is given, there are $2n + 2$ variables in the overall system, that is, x_i, N_i, ϕ_{el} and ϕ_{ion}. The coupled overall MEA model can be solved by using the commercial software ***FEMLAB***. Then, the operating current density can be obtained from the post processing

$$I = \sigma_{ion} \frac{d\phi_{ion}}{dz}\Big|_{z=l_a}^{+} \tag{13}$$

Validation and Simulation

Base case and model validation

Table 1 lists part of the structural parameters of the experimental cell and the operating conditions in the base case.[14] Here, 85%H_2–15%H_2O binary mixture is used as fuel and air is used as oxidant.

The experimental cell is an anode-supported button solid-oxide fuel cell which focuses on the problem of mass transfer and electrochemical reaction, and is usually used to mask the phenomena of flow and heat transfer. Corresponding to the small effective cell area (1.1 cm^2), and the fuel and air flow rate (140 mL/min, 550 mL/min, respectively), it allows us to use the inlet gas concentration as the bulk-gas concentration directly under the low fuel and air utilization. Table 2 lists the interpolation parameters of the general model in the base case.

Table 2. Basic Parameters in the General MEA Model

Parameter	Symbol	Value
Anode porosity/tortuosity	$\varepsilon_{p,a}/\tau_a$	0.1
Cathode porosity/tortuosity	$\varepsilon_{p,c}/\tau_c$	0.1
H_2 reference exchange current density (A/m^2)	$i_{0,H_2,ref}$	3435.4
O_2 reference exchange current density (A/m^2)	$i_{0,O_2,ref}$	1557.7
Anode TPB specific area (m^2/m^3)	$S_{TPB,a}$	2×10^5
Cathode TPB specific area (m^2/m^3)	$S_{TPB,c}$	2×10^5
Anodic transfer coefficient in anode[15]	α_a	1.0
Cathodic transfer coefficient in anode[15]	β_a	0.5
Anodic transfer coefficient in cathode[15]	α_c	0.5
Cathodic transfer coefficient in cathode[15]	β_c	0.5
H_2 reaction order[15]	γ_{H_2}	0.734
H_2O reaction order[15]	γ_{H_2O}	0.266
O_2 reaction order	γ_{O_2}	0.25
Ionic phase conductivity (S/m)[16]	σ_{ion}	$3.34 \times 10^4 . \exp(-10300/T)$
Anode electronic phase conductivity (S/m)[16]	$\sigma_{el,a}$	$9.5 \times 10^7/T . \exp(-1150/T)$
Cathode electronic phase conductivity (S/m)[16]	$\sigma_{el,c}$	$4.2 \times 10^7/T . \exp(-1200/T)$

Figure 2 shows the comparison between the experimental polarization cure and the simulation results. In the base case, there is a good prediction of the general model where the open circuit voltage is derived from the real measurement instead of the Nernst equation. The distribution among the anode overpotential, cathode overpotential, and the ohmic loss is also shown in Figure 2. Although the anode is much thicker than the cathode, the cathode overpotential is still the dominant polarization because of the high H_2 concentration in the H_2-H_2O fuel system.

Effects of fuel component and anode porosity/tortuosity

The general MEA model can be used to analyze the effects of the structural parameters (electrode porosity, tortuosity and thickness, TPB active area per unit volume, etc), and the operating parameters (gas pressure, temperature and concentration, etc) on the cell performance. In this article, it is focused on the effects of the fuel component and the ratio of the anode porosity to tortuosity.

Figure 3 shows the comparison between the experimental cell performance and the simulation results under the different fuel components of H_2—H_2O system. Besides the inlet fuel concentration, other parameters are the same as that in the base case. As shown in Figure 3, when the hydrogen-bulk concentration decreases, the hydrogen concentration at the triple-phase boundary decreases, and the anode overpotential increases. When the inlet hydrogen molar fraction is low, there is an obvious section of concentration polarization in the *V-I* performance curve. As the TPB hydrogen concentration decreases to zero, the operating current density reaches the limiting current density. In this critical condition, there is great discrepancy between the prediction of the general MEA model and the experimental data.

The ratio of electrode porosity to tortuosity plays an important role in the gas transfer in the porous electrode. In

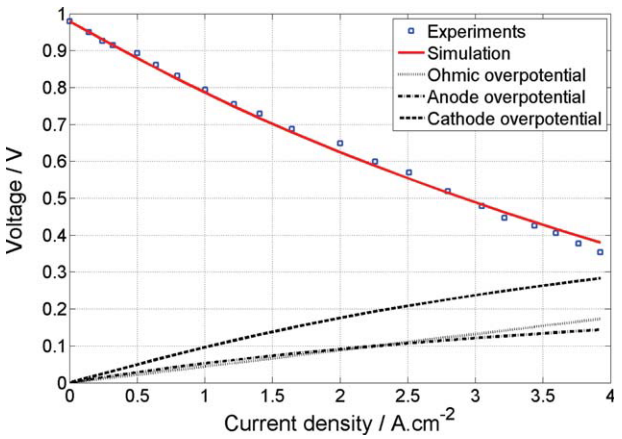

Figure 2. Validation of the general MEA model in the base case, i.e., 85%H_2–15%H_2O binary mixture is used as fuel.

[Color figure can be viewed in the online issue, which is available at www.interscience.wiley.com.]

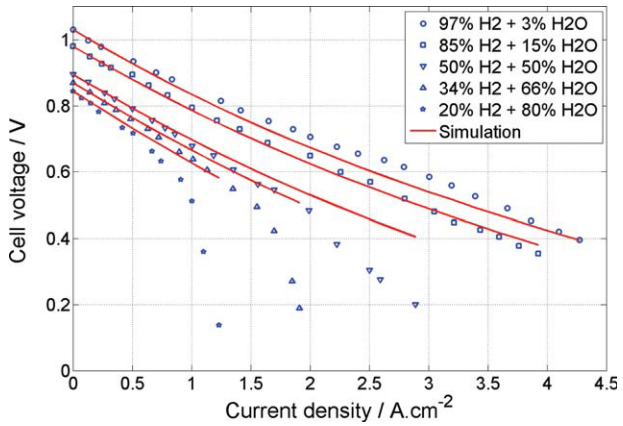

Figure 3. Comparison between the experimental data and the simulation results of the general MEA model under the different fuel components of H_2—H_2O system.

The anode porosity/tortuosity is equal to 0.1 ($\varepsilon_p/\tau = 0.1$). [Color figure can be viewed in the online issue, which is available at www.interscience.wiley.com.]

Eq. 4, the effective gas-binary diffusivity and Kundsen diffusivity in the electrode is corrected by multiplying the corresponding diffusion coefficient with the electrode porosity/tortuosity. As mentioned previously, at low-fuel concentration or high-fuel utilization, it is hard for the general MEA model to completely describe the diffusion resistance, which usually leads to overestimation of the cell performance. Thus, the variable anode tortuosity is generally used to solve the problem in the general MEA model. That is to increase the anode tortuosity at the low-fuel concentration, as, thus, the effective gas bulk and Kundsen diffusivity is decreased while the diffusion resistance is increased. As shown in Figure 4, by modifying the value of the anode porosity/tortuosity to a low level ($\varepsilon_p/\tau = 0.033$), there is a good prediction of the general MEA model in different H_2—H_2O components. Compared to the value of $\varepsilon_p/\tau = 0.1$ in the base case (as shown in Figure 3), the anode porosity/tortuosity has an obvious effects on the cell performance.

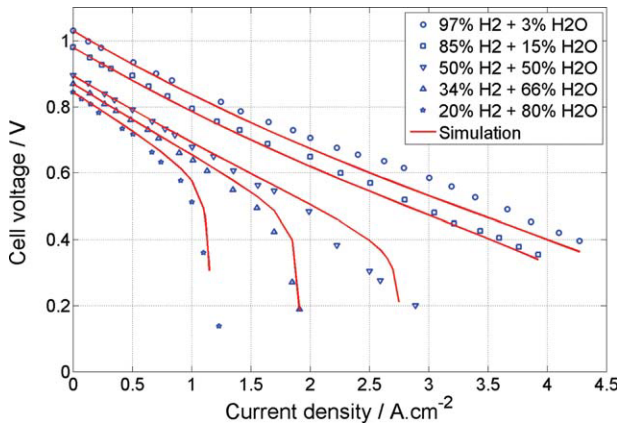

Figure 4. Comparison between the experimental data and the simulation results of the general MEA model under the different fuel components of H_2—H_2O system.

For interpolation, the anode porosity/tortuosity is modified to 0.033 ($\varepsilon_p/\tau = 0.033$). [Color figure can be viewed in the online issue, which is available at www.interscience.wiley.com.]

Advanced MEA model

As mentioned previously, at high-operating current density or high-fuel utilization, the variable anode porosity/tortuosity is needed for the good prediction of the general MEA model. However, the anode porosity and tortuosity are both the cell structural parameters, which should be independent on the operating conditions. In most SOFC characterization, the electrode tortuosity is within the range of 2–6.[17] In Figure 4, the value of $\varepsilon_p/\tau = 0.033$ means the value of $\tau = 15$ corresponding to $\varepsilon = 0.5$, which is obviously unreasonable.

Diffusion equivalent circuit and correction of TPB gas concentration

According to the theory of heterogeneous catalysis, mass transfer, electrochemical and chemical reaction of fuel mixture in the porous anode includes multiple elementary steps of gas diffusion, absorption and desorption, which can be considered as two basic processes as follows:

1. The fuel reactants diffuse from the flow channel to the sites adjacent to the triple phase boundary via the anode pore. This process includes the gases' molecular diffusion, Knudsen diffusion and the convective mass transfer because of the pressure difference. In the general MEA model, it has been described by the Stefan-Maxwell equation or the dusty gas model.

2. From the sites adjacent to TPB, the fuel species reach the TPB and react with the oxygen ion. At the low-operating current density or the low-fuel utilization, there are plenty of the active reaction sites where the surface diffusion and absorption competition of species are negligible. However, in the ciritical conditions, most of the active reaction sites are occupied by the absorbed fuel and product species. In this case, the competitive absorption between gaseous species and the surface diffusion from the absorbed sites to TPB becomes the dominant factor.

So the general MEA model should be improved by introducing the mechanism of surface diffusion and competitive absorption. In Williford's work,[17] the resistances of bulk diffusion and the surface diffusion are considered as parallel at the low-operating current density, and serial at the high-operating current density. In this regard, a series-connection diffusion equivalent circuit model is introduced to correct

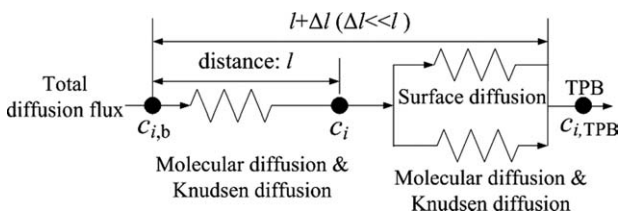

Figure 5. Diffusion equivalent circuit for the correction of the TPB gas concentration.

the gas concentration at TPB.[18] As shown in Figure 5, $c_{i,b}$ is the bulk concentration of species i at the anode/flow channel interface, c_i is the local intrinsic concentration at the site adjacent to TPB, and $c_{i,TPB}$ is the real concentration for the electrochemical reaction at TPB by taking the surface diffusion into account.

According to the theory of Langmuir isothermal absorption, the surface coverage of species i at the Ni surface of the anode, θ_i is

$$\theta_i = \frac{b_i p_i}{1 + \sum_i b_i p_i} \tag{14}$$

where p_i is the partial pressure of species i, b_i is the Langmuir parameter

$$b_i = \frac{N_A \pi r_i^2 \tau_0}{\sqrt{2\pi \Re T M_i}} \exp(Q_i / \Re T) \tag{15}$$

where N_A is Avogadro's number, r_i and M_i is the molecular radius and molecular weigh of species i, respectively, τ_0 is the vibrational period (10^{-13} s), and Q_i is the activation energy for adsorption.

In general, the value of θ_i is small at the high-operating temperature of SOFC. The relative surface coverage of species i, Θ_i is used here instead of the absolute coverage[17]

$$\Theta_i = \theta_i \Big/ \sum\nolimits_i \theta_i \tag{16}$$

The total diffusion coefficient of species i, $D_{i,t}$ is the product of exponent weighted bulk diffusion D_i and surface diffusion coefficient $D_{s,i}$ with the relative coverage Θ_i[17]

$$D_{i,t} = D_i^{\Theta_i} D_{s,i}^{1-\Theta_i} \tag{17}$$

The aforementioned equation means the bulk diffusion is dominant when the relative coverage is high and the surface diffusion is dominant when the relative coverage is low. This equation should only be used for the correction of diffusivities of reactant species (H_2, CO). The product and inert species (H_2O, CO_2, N_2) just affect the relative coverage via competitive absorption. For the gaseous mixture, the bulk diffusivity can be approximated by

$$D_i = (1 - x_i) \Big/ \sum_{j \neq i} (x_j / D_{ij}) \tag{18}$$

The surface diffusion coefficient can be described by[17]

$$D_{s,i} = \frac{D_{s,i,0}^{1-\Theta_i} D_{s,i,1}^{\Theta_i}}{1 - \Theta_i} \tag{19}$$

where $D_{s,i,0}$ and $D_{s,i,1}$ is the surface diffusion coefficient at zero coverage ($\Theta_i \approx 0$) or full coverage ($\Theta_i \approx 1$), respectively. In general, $D_{s,i,1} \ll D_{s,i,0}$.

According to the diffusion equivalent circuit and the linear Fick's law, there is

$$D_{i,t} \frac{c_{i,b} - c_{i,TPB}}{l + \Delta l} = D_i \frac{c_{i,b} - c_i}{l} \tag{20}$$

Table 3. Surface Diffusion Parameters for H_2—H_2O System

Parameter	Symbol	Value
H_2 activation energy for absorption (eV/molecule)	Q_{H_2}	0.45
H_2O activation energy for absorption (eV/molecule)	Q_{H_2O}	0.5
H_2 surface diffusivity at zero coverage/effective H_2—H_2O binary diffusivity	$\frac{D_{s,H_2,0}}{D_{H_2,H_2O}} \frac{\tau}{\varepsilon_P}$	1/2
H_2 surface diffusivity at full coverage/effective H_2—H_2O binary diffusivity	$\frac{D_{s,H_2,1}}{D_{H_2,H_2O}} \frac{\tau}{\varepsilon_P}$	1/200

where l is the distance of bulk diffusion, Δl is the distance of surface diffusion. Considering $l \gg \Delta l$, the species concentration at TPB can be obtained by

$$c_{i,TPB} = c_{i,b} - (D_i / D_{s,i})^{1-\Theta_i} (c_{i,b} - c_i) \tag{21}$$

Substitute Eq. 21 into the general current-overpotential equation (Eq. 2), it forms the advanced MEA model which keeps the same simple structure and boundary conditions as that of the general MEA model.

Validation and simulation

Compared to the general MEA model, there are some additional parameters ($D_{s,i,0}$, $D_{s,i,1}$ and Q_i) in the advanced MEA model. Table 3 lists the fitted parameters for H_2—H_2O system.

For the binary fuel system, it is found that the increment of fuel (H_2 or CO) adsorption activation energy or the decrement of product (H_2O or CO_2) adsorption activation energy leads to better cell performance. On the other hand, the concentration overpotential increases as the surface diffusivities decrease. As a first approximation, the adsorption activation energies can be taken as 0.5 eV/molecule. The fitted values of $Q_{H_2} = 0.45$ eV/molecule and $Q_{H_2O} = 0.5$ eV/molecule are in good agreement with the data of $Q_{H_2} = 0.425$ eV/molecule[17] and $Q_{H_2O} = 0.539$ eV/molecule of H_2O desorption energy on the clean Ni(111) surface.[19] In general, the surface diffusivity of H_2 or CO at low coverage is in the rage of 0.01–1 cm^2/s and in the same order of the bulk diffusivity. At the operating temperature, $T = 1073.5$ K, there is $D_{H_2,H_2O} = 8$ cm^2/s, $\varepsilon_p/\tau = 0.1$, and the fitted value of $D_{s,H_2,0} = 0.4$ cm^2/s. Although the fitted value of $D_{s,H_2,1} = 4 \times 10^{-3}$ cm^2/s slightly deviates from the experimental data of $4.8–6.8 \times 10^{-4}$ cm^2/s for H_2 on Ni(100),[20] the ratio between the low-coverage and high-coverage surface diffusivities, $D_{s,H_2,0}/D_{s,H_2,1} = 100$ is in good agreement with the fitted data of $D_{s,H_2,0}/D_{s,H_2,1} = 191.5$.[17]

Figure 6 shows the comparison between the experimental polarization cure and the simulation results of the advanced MEA model. Via introduction of the mechanism of competitive absorption and surface diffusion, there is good prediction of the advanced MEA model with the fixed value of the anode porosity/tortuosity ($\varepsilon_p/\tau = 0.1$) at the different components for H_2—H_2O binary fuel system. Figure 7 shows the variation of hydrogen coverage and molar fraction at the anode/electrolyte interface when the current density varies.

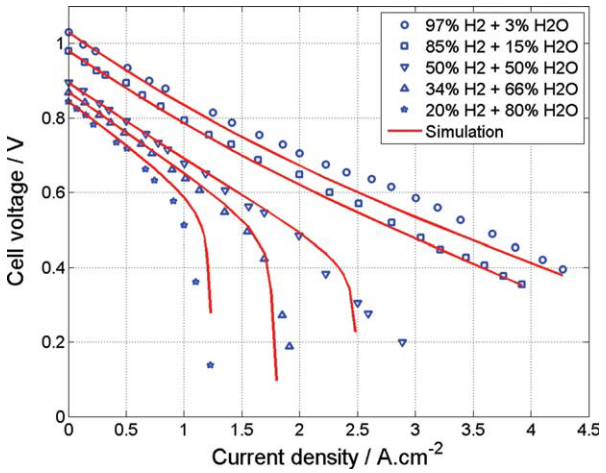

Figure 6. Validation of the advanced MEA model under the different fuel components of H_2—H_2O binary system.

The anode porosity/tortuosity is kept to 0.1 ($\varepsilon_p/\tau = 0.1$). [Color figure can be viewed in the online issue, which is available at www.interscience.wiley.com.]

Similar to the hydrogen molar fraction, the hydrogen coverage decreases as the current density increases.

Similar to the H_2—H_2O system, Table 4 lists the fitted parameters for CO—CO_2 binary fuel system. The fitted value of $Q_{CO} = 0.975$ eV/molecule, $Q_{CO_2} = 0.825$ eV/molecule are in good agreement with the experimental data of $Q_{CO} = 0.94$–1.92 eV/molecule[21] and $Q_{CO_2} = 0.35$–0.74 eV/molecule.[22] At the operating temperature, $T = 1073.5$ K, there is $D_{CO,CO_2} = 1.54$ cm^2/s, $\varepsilon_p/\tau = 0.1$, and the fitted value of $D_{s,CO,0} = 0.077$ cm^2/s is in the same order of the bulk diffusivity. With the same ratio between two surface diffusivities, $D_{s,CO,0}/D_{s,CO,1} = 100$, the value of high-coverage surface diffusivity, $D_{s,CO,1} = 7.7 \times 10^{-4}$ cm^2/s is in good agreement with the experimental data of 0.41–4.9×10^{-4} cm^2/s.[20] As shown in Figure 8, the advanced MEA model is also validated by the experimental data at different CO—CO_2 fuel components.[14]

Table 4. Parameters for CO—CO_2 Binary Fuel System

Parameter	Symbol	Value
CO reference exchange current density (A.m^{-2})	$i_{0,CO,ref}$	60
CO reaction order	γ_{CO}	1.65
CO_2 reaction order	γ_{CO_2}	0
CO activation energy for absorption (eV/molecule)	Q_{CO}	0.975
CO_2 activation energy for absorption (eV/molecule)	Q_{CO_2}	0.825
CO surface diffusivity at zero coverage/effective CO—CO_2 binary diffusivity	$\frac{D_{s,CO,0}}{D_{CO,CO_2}}\frac{\tau}{\varepsilon_p}$	1/2
CO surface diffusivity at full coverage/effective CO—CO_2 binary diffusivity	$\frac{D_{s,CO,1}}{D_{CO,CO_2}}\frac{\tau}{\varepsilon_p}$	1/200

For further validation, the advanced MEA model was also used for the prediction of cell performance at H_2—H_2O—CO—CO_2 fuel mixture system. At this time, there is water-gas-shift chemical reaction (CO + H_2O → H_2 + CO_2) in the anode, and the kinetics (mol/m^3.s) in the Ni-YSZ cermet can be obtained by[23]

$$r_{shift} = 0.0171\exp\left(-\frac{103191}{\Re T}\right)\left(p_{CO}p_{H_2O} - \frac{p_{H_2}p_{CO_2}}{K_{eq,shift}}\right) \quad (22)$$

$$K_{eq,shift} = \exp\left(-0.2935Z^3 + 0.635Z^2 + 4.1788Z + 0.3169\right) \quad (23)$$

where $Z = 1{,}000/T - 1$. Then the chemical reaction rate of species i in Eq. 5 is $R_i = \upsilon_{shift,i}r_{shift}$, in which $\upsilon_{shift,i}$ is the stoichiometric coefficient of water-gas shift reaction.

With the same parameters in Table 1–4, Figure 9 shows the comparison among the experimental polarization curve,[14] and the simulation results of the general and the advanced MEA model at H_2—CO fuel system. Obviously, the advanced

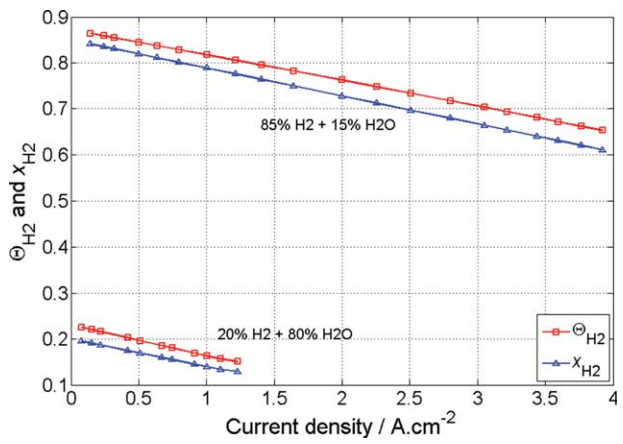

Figure 7. Hydrogen relative coverage and molar fraction at the anode/electrolyte interface with the variation of current density.

[Color figure can be viewed in the online issue, which is available at www.interscience.wiley.com.]

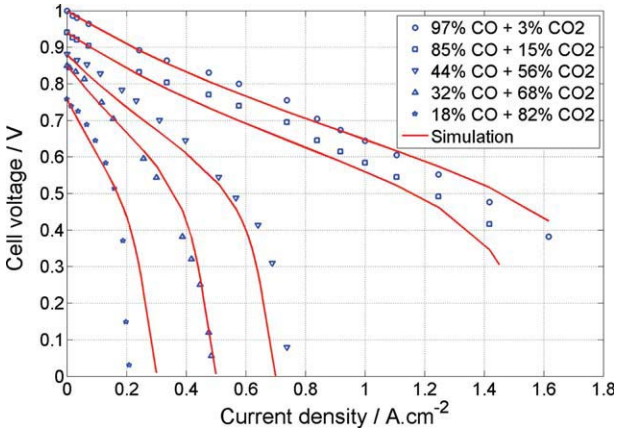

Figure 8. Validation of the advanced MEA model under the different fuel components of CO—CO_2 binary system.

The anode porosity/tortuosity is kept to 0.1 ($\varepsilon_p/\tau = 0.1$). [Color figure can be viewed in the online issue, which is available at www.interscience.wiley.com.]

MEA model prevails at the low inlet H_2 concentration. However, as shown in Figure 10, there is also obvious discrepancy between the prediction of the advanced MEA model and the experimental data at the low H_2 inlet molar fraction for H_2—CO_2 fuel system.[14]

Conclusion

Describing the mass transfer and electrochemical reaction in the membrane electrode assembly (MEA) is the core of modeling of solid oxide fuel cell (SOFC). Compared to the analysis of complex heterogeneous elementary steps, the general MEA model has the simple structure which has been widely used for cell-level and system-level simulation. However, it often overestimates the cell performance at high-current density or high-fuel utilization, which usually stands out at the downstream part of the cell and the staged stack as the fuel is consumed and diluted.

In order to fit the polarization data at the section of concentration loss, the variable electrode tortuosity is used in the general MEA model to artificially decrease the effective gas-bulk diffusivity and increase the resistance of mass transfer at the low-fuel concentration. However, the porosity and tortuosity are both the electrode structural parameters which should be independent of the operating conditions.

In this article, an advanced MEA model was developed to improve the accuracy of general PEN-level models at high-fuel utilization. Based on the diffusion equivalent circuit model, the mechanisms of surface diffusion and competition absorption were introduced to reflect the overall resistance of mass transfer. Via the simple correction of the species concentrations at TPBs, the same structure and boundary conditions of the general MEA models is kept in the advanced MEA model. Thus, good prediction of cell performance in a wide range can be obtained with the negligible increment in computational time. Thus, the decrement of effective gas diffusivity via unreasonable increment of the electrode tortuosity in the general MEA model can be avoided. The advanced MEA model in this article has been validated in the cases of different fuel components for H_2–H_2O, CO–CO_2, and H_2–CO fuel system. By comparison between the cell performance of 20%H_2–80%H_2O fuel system as shown in Figures 3 and 6, the maximum relative error is reduced from 316% in the general model to 110% in the advanced model.

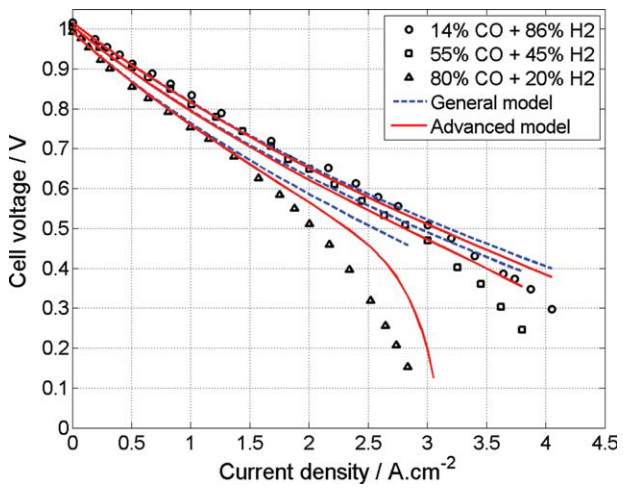

Figure 9. Validation of the advanced MEA model under the different fuel components of H_2-CO mixture system.

The anode porosity/tortuosity is kept to 0.1 ($\varepsilon_p/\tau = 0.1$). [Color figure can be viewed in the online issue, which is available at www.interscience.wiley.com.]

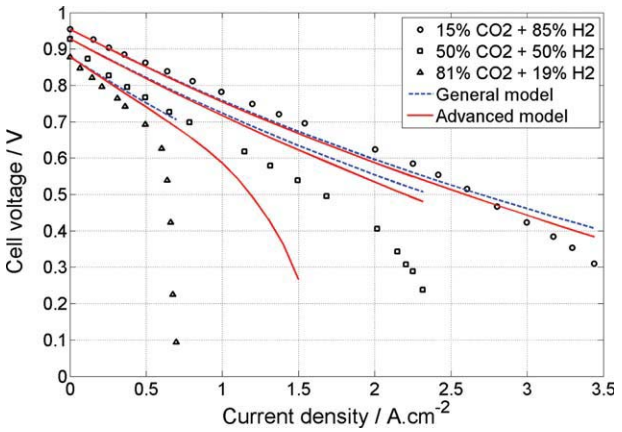

Figure 10. Validation of the advanced MEA model under the different fuel components of H_2—CO_2 mixture system.

The anode porosity/tortuosity is kept to 0.1 ($\varepsilon_p/\tau = 0.1$). [Color figure can be viewed in the online issue, which is available at www.interscience.wiley.com.]

However, there are also significant discrepancy between the prediction of the advanced model and the experimental results at the low H_2 concentration of H_2-CO_2 fuel system. The key point is probably due to the intrinsic structure of the electrochemical model in the homogeneous MEA models. As mentioned previously, there are various expressions of the exchange current density, reaction orders of reactants and products, etc. A good solution is to obtain the modified Bulter-Volmer equation and expression of the current density by assuming the rate-determining step in the elementary model.[11] However, the elementary analysis of the multicomponent fuel mixture based on the suitable reaction pathway is complex and will be our next work.

Acknowledgments

Financial support from Natural Science Foundation (Project No. 50706019) is gratefully acknowledged.

Notation

c = concentration, mol/m^3
D = diffusivity, m^2.s
E = activation energy for electrochemical reaction, J/mol
F = Faraday's constant, 96487 C/mol
i_0 = exchange current density, A/m^2
i = local current density, A/m^2
I = operating current density, A/m^2
j = electrochemical reaction rate, A/m^3
l = thickness, m
M = molecular weight, kg/mol
n_e = electrons transferred per reacting molecule, $n_e = 2$
N = flux, mol/m^2.s

p = pressure, Pa
Q = activation energy for surface adsorption, J/mol
r_{shift} = kinetics of water gas shift reaction, mol/m^3.s
R = chemical reaction rate, mol/m^3.s
$\Re$ = universal gas constant, 8.314 J/mol.K
S_{TPB} = active area of triple-phase boundary (TPB) per unit volume (m^2/m^3)
T = temperature, K
V_{cell} = cell voltage, V
x = molar fraction
z = spatial coordinate along the electrode thickness, m

Greek letters

α = anodic-transfer coefficient
β = cathodic-transfer coefficient
ε_p = electrode porosity
η = overpotential, V
γ = reaction order
ϕ = potential, V
σ = conductivity, S/m
τ = electrode tortuosity
θ = absolute surface coverage
Θ = relative surface coverage
υ = stoichiometric coefficient of reaction

Subscripts and superscripts

a = anode
c = cathode
e = electrolyte
eff = effective
el = electronic conducting phase
eq = equilibrium
K = Knudsen
i, j = species
ion = Ionic conducting phase
ref = reference
t = total or overall
TPB = triple-phase boundary

Literature Cited

1. Bao C, Cai NS. Research status and advances in modeling and control of solid oxide fuel cell-gas turbine hybrid generation system (in Chinese). *Chin J Mech Eng*. 2008;44(2):1–7.
2. Costamagna P, Costa P, Antonucci V. Micro-modelling of solid oxide fuel cell electrodes. *Electrochimica Acta*. 1998;43:375–394.
3. Xia ZT, Chan SH, Khor KA. An improved anode micro model of SOFC. *Electrochem Solid-State Lett*. 2004;7(3):A63–A65.
4. Kim JW, Virkar AV, Fung KZ, Mehta K, Singhal SC. Polarization effects in intermediate temperature, anode-supported solid oxide fuel cells. *J Electrochem Soc*. 1999;146:69–78.
5. Chan SH, Khor KA, Xia ZT. A complete polarization model of a solid oxide fuel cell and its sensitivity to the change of cell component thickness. *J Power Sources*. 2001;93:130–140.
6. Suwanwarangkul R, Croiset E, Fowler MW, Douglas PL, Entchev E, Douglas MA. Performance comparison of Fick's, dusty-gas and Stefan-Maxwell models to predict the concentration overpotential of a SOFC anode. *J Power Sources*. 2003;122:9–18.
7. Hussain MM, Li X, Dincer I. Multi-component mathematical model of solid oxide fuel cell anode. *Int J Energy Res*. 2005;29:1083–1101.
8. Aloui T, Halouani K. Analytical modeling of polarizations in a solid oxide fuel cell using biomass syngas product as fuel. *Appl Therm Eng*. 2007;27:731–737.
9. Bieberle A, Gauckler LJ. State-space modeling of the anodic SOFC system Ni, H_2—H_2O|YSZ. *Solid State Ionics*. 2002;146:23–41.
10. Bessler WG. A new computational approach for SOFC impedance based on detailed electrochemical reaction-diffusion models. *Solid State Ionics*. 2005;176:997–1011.
11. Zhu H, Kee RJ, Janardhanan VM, Deutschmann O, Goodwin DG. Modeling elementary heterogeneous chemistry and electrochemistry in solid-oxide fuel cells. *J Electrochem Soc*. 2005;152(12):A2427–A2440.
12. Bao C, Cai NS. An approximate analytical solution of transport model in electrodes for anode-supported solid oxide fuel cells. *AIChE J*. 2007;53(11):2968–2979.
13. Poling BE, Prausnitz JM, O'Connell JP. *The Properties of liquids and gases*. 5th ed. New York: McGraw-Hill; 2000.
14. Jiang Yi, Virkar AV. Fuel composition and diluent effect on gas transport and performance of anode-supported SOFCs. *J Electrochem Soc*. 2003;150(7):A942–A951.
15. Nagata S, Momma A, Kato T, Kasuga Y. Numerical analysis of output characteristics of tubular SOFC with internal reformer. *J Power Sources*. 2001;101:60–71.
16. Ferguson JR, Fiard JM, Herbin R. Three-dimensional numerical simulation for various geometries of solid oxide fuel cells. *J Power Sources*. 1996;58:109–122.
17. Williford RE, Chick LA, Maupin GD, Simmer SP, Stevenson JW. Diffusion limitations in the porous anodes of SOFCs. *J Electrochem Soc*. 2003;150:A1067–A1072.
18. Shi YX, Cai NS, Li C. Numerical modeling of an anode-supported SOFC button cell considering anodic surface diffusion. *J Power Sources*. 2007;164:639–648.
19. Schulze M, Reissner R, Bolwin K, Kuch W. Interaction of water with clean and oxygen precovered nickel surfaces. *Fresenius J Anal Chem*. 1995;353:661–665.
20. Seebauer EG, Allen CE. Estimation surface diffusion coefficients. *Prog Surface Sci*. 1995;49:265–330.
21. Shah V, Li T, Baumert KL, Cheng HS, Sholl DS. A comparative study of CO chemisorption on flat and stepped Ni surfaces using density functional theory. *Surface Sci*. 2003,537:217–227.
22. Wang SG, Cao DB, Li YW, Wang JG, Jiao HJ. Chemisorption of CO_2 on nickel surfaces. *J Phys Chem B*. 2005;109:18956–18963.
23. Haberman BA, Young JB. Three-dimensional simulation of chemically reacting gas flows in the porous support structure of an integrated-planar solid oxide fuel cell. *Int J Heat Mass Transfer*. 2004;47:3617–3629.

Manuscript received Sept. 13, 2008, and revision received July 27, 2009.